

Short Communication

Electrodeposition of ZnO Film With Enhanced Photocatalytic Activity Towards Methylene Blue Degradation

Feng Zhang^{1,*}, Wenjuan Zhang², Xiaolin Luo¹, Guodong Feng¹ and LiFang Zhao¹

¹ Key laboratory of Advanced molecular engineering materials; Department of Chemistry and Chemical Engineering, Baoji University of Arts and Science, Baoji, Shaanxi, 721013, P.R. China

² Department of Electrical Engineering, Baoji University of Arts and Sciences, Shaanxi, 721013, P.R. China

*E-mail: bj_zhangfeng@yeah.net

Received: 14 February 2017 / Accepted: 8 March 2017 / Published: 12 April 2017

A moderate electrodeposition synthesis was developed in this work to prepare a ZnO film. The target of this research is to determine the best photoelectrochemical response for solar-induced water decomposition. On the basis of the acquired results, a nanostructured ZnO film was developed on the surface of a substrate. The photocatalytic and photoelectrochemical responses of the obtained wurtzite-type ZnO film were monitored and assessed for comparison with those of the commercial ZnO. In respect to the newly formed ZnO thin film, light current densities of 17.14 mA/cm² under ultraviolet light and 13.71 mA/cm² under visible light were observed. The ZnO film was believed to possess excellent capacity to absorb more incident photons from the illumination to produce more photoinduced charge carriers, giving rise to the photocatalytic and photoelectrochemical reactions. In addition, incident rays from any orientation can be caused by light-scattering effects and the high specific surface area of 2D nanostructures.

Keywords: Electrodeposition; ZnO; Photocatalysis; Thin film; Methylene blue; Organic waste

1. INTRODUCTION

Photocatalytic degradation has attracted the attention of many people due to its high potential to promote the decay of organic pollutants in sewage water. Compared with the traditional method, it is found to possess several merits, including reacting rapidly, degrading pollutants, operating in a moderate reaction environment and having easy accessibility. To date, a variety of semiconductor nanopowders, such as TiO₂ [1], SnO₂ [2], WO₃ [3] and ZnO [4, 5], are believed to be excellent light catalysts for sewage water disposal owing to their proper energy bandgap and high specific surface area.

Zinc oxide (ZnO), an II–VI compound semiconductor whose band gap is high (namely, 3.37 eV at room temperature) is generally believed to be one of the most promising substances for applications related to environmental protection, such as air cleaning, water cleaning and the remediation of harmful waste [6-11]. At present, there primarily two major means for the development of ZnO nanostructures, namely, liquid-phase and gas-phase syntheses. With the purpose of improving the photocatalytic properties of ZnO nanostructures to the largest extent possible, much work has been done in order to perfect the synthesis approach for the controlled development and assembly of the ZnO nanostructures. Moreover, many morphologies have already been made, e.g., nanowires [12-14], nanorods [15], nanorings, nanobows [16], nanoneedles [17], nanopins [18], nanoflowers [19, 20], nanobelts [21], rotor-like [21] and obelisk-like [22] structures. ZnO nanostructures have been adopted to realize the degradation of a variety of organic chemicals [23, 24]. Nonetheless, these ZnO photocatalysts are found to be difficult to recover for use in diverse applications [25]. To figure out the issues related to the segregation and recovery of nanostructured ZnO photocatalysts, complicated ZnO nanostructures been synthesized on a substrate. For instance, layered ZnO nanostructures on a variety of substrates have been made through successive nucleations, as well as through a multistep solid-state synthesis approach [26]. What should be emphasized is that the redundant multistep process adversely affects being able to apply the material broadly. Single-crystal ZnO nanorod arrays as well as ZnO pine nanotrees, whose branches very much resemble nanoblades, were formed on the surface of a Zn substrate, and their characteristic photocatalytic activities were revealed in this process. [27]. Based on an in-depth analysis, it was found that photocatalytic activity of ZnO for the realization of organic pollutants' degradation largely relies on the photocatalytically active ZnO [001] facet. Nevertheless, at present, the control of the polar [001] facet of ZnO photocatalyst is still challenging, which has restricted the photocatalytic activity of ZnO and its practical use [28]. Owing to this limitation, it is extremely necessary to develop a moderate approach at macroscale and with a low cost in order to realize the fabrication of well-defined ZnO nanostructured films characterized by large surface areas and a high proportion of the exposed polar [001] facet.

In this study, an electrodeposition technique was developed with the purpose of preparing nanostructured ZnO films on ITO that could guarantee the control of the polar [001] facet of ZnO. Initially, ZnO nanostructures exist within ITO. By means of the degradation of methylene blue (MB) under ultraviolet radiation, the photocatalytic activities of the nanostructured ZnO films were studied. On account of its large surface area, as well as its high proportion of the exposed polar [001] facet, the porous ZnO film formed on nanosheets revealed outstanding photocatalytic activity.

2. EXPERIMENTS

2.1. Chemicals

In this study, all chemical reagents were of analytical quality and used without any further purification. In addition, deionized water was used in the preparation of all aqueous solutions. ZnO seeds' precursors contained a zinc acetate colloid obtained through the dissolution of zinc acetate dehydrate and ethanolamine in a 1:1 molar ratio in 2-methoxyethanol, with stirring for half an hour at 60 °C. Commercial ZnO powder was purchased from Sigma-Aldrich.

2.2. Preparation of ZnO film

Electrodeposition of ZnO films was carried out using an electrochemical analytical workstation (CHI 760C) with a typical three-electrode arrangement. In this process, the working electrode was the ITO, whereas the counter and reference electrodes were a Pt wire and saturated calomel electrode (SCE), respectively. In addition, the electrolyte was a ZnCl₂ aqueous solution overflowing with saturated O₂ throughout the course of the reaction, and at the same time, KCl (0.1 M) was added into the solution as the supporting electrolyte. The electrochemical cell was placed at 80 °C, while the potential was set at -1.0 V vs. SCE for 1800 s. It was found that hydroxide ions developed at the ITO surface through the reduction of an oxygen precursor that generated a chemical reaction with Zn²⁺ ions inside the solution, giving rise to Zn(OH)_x^{2-x}. Then, through the autonomous water removal of Zn(OH)_x^{2-x}, ZnO particles were formed accordingly on the working electrode. To form a ZnO film with great growth density, the ITO was handled in the following manner: first, it was soaked in the 0.75 M zinc acetate colloid for a fixed period; second, it annealed in the air for 5 minutes at 350 °C to acquire a film of identical ZnO nanoseeds; third, after sedimentation, the nanostructured ZnO layer was annealed for 3 hours at 600°C.

2.3. Characterization

To characterize the surface morphologies of the ZnO layer fabricated in advance, a field emission scanning electron microscope (FESEM, Zeiss Supra-55, operated at 10 kV) was employed. With a powder X-ray diffractometer (Rigaku Dmax-2500 diffractometer utilizing Cu K α radiation), the measurement of X-ray diffraction (XRD) patterns was achieved. In addition, the measurement of the ultraviolet and visible (UV-vis) absorption spectrum was done with the use of a double beam UV-vis spectrophotometer (provided by Beijing Purkinje General Instrument Co., Ltd., TU-1901), using BaSO₄ as the background and developing the baseline from 230 nm to 900 nm. To study the photocurrent density of the sample, a three-electrode PEC quartz cell was filled with 1 M sodium hydroxide (NaOH) containing 1 v% of ethylene glycol. A nanodisk-dendritic ZnO film served as the anode, a platinum rod served as the cathode, and a saturated calomel electrode (SCE) served as the reference electrode. A 150-W xenon lamp (Zolix LSP-X150) was set to focus on the immersed portion of the photoelectrode to simulate solar irradiation. The three electrodes were connected to the potentiostat (MetrohmAutolab PGSTAT204), and the current-voltage values were measured.

2.4. Measurements of photocatalytic activities

The measurement of the photocatalytic desaturation of the MB water solution under ultraviolet light ($I_0 = 134 \mu\text{W cm}^{-2}$) using ZnO films was conducted at indoor temperature. The procedure of the experiments could be summarized as follows: the ZnO layers were soaked inside a quartz reactor in which there was 10 mL of a 1×10^{-5} M aqueous MB solution. Subsequently, this reactor was placed approximately 10.0 cm away from the ultraviolet ray source with the purpose of lessening the heat effect of the rays to the largest degree. When the irradiation was occurring, the MB solution's

concentration was successfully measured and recorded at 30-min intervals with the use of a UV-vis spectrophotometer (Unico UV-4802H). For the precise assessment of the photocatalytic ZnO film's recycling as well as recovery, the photocatalytic desaturation process was carried out 10 times. When this process was finished, the ZnO film was cleaned by using deionized water in order to remove the remaining MB. After this step, the ZnO film was soaked inside a newly formed solution that had the same concentration of MB in order to repeat the photocatalytic degradation experiment.

3. RESULTS AND DISCUSSION

Of the performed tests, XRD analysis was adopted to determine the crystallinity of the original ZnO thin film and of the obtained ZnO thin film, and the results are clearly shown in Figure 1. As shown in Figure 1A, the XRD pattern of the resultant ZnO thin film mostly reveals a Zn phase, signifying that there were amorphous characteristics. The Bragg reflections of the Zn phase could be observed at values of 36.32, 39.04, 43.21, 54.37, 70.04, 70.62, and 77.05° in the XRD patterns, which correspond to the (002), (100), (101), (102), (013), (110), and (004) crystal planes, respectively. The fact that the Zn phase existed was proven by the ICDD file of 00-004-0831. With respect to ZnO thin film, as revealed in Figure 1B, the outcome indicates that the specimens are consistent with reference code ICDD 00-036-1451, revealing the ZnO phase. For the ZnO phase, its Bragg reflections could be observed at values of 31.71, 34.53, 36.34, 47.62, 62.26, 66.43, 67.91, 70.05, and 77.2° in the XRD patterns, which correspond to the (100), (002), (101), (102), (103), (200), (112), (004), and (202) crystal planes, respectively.

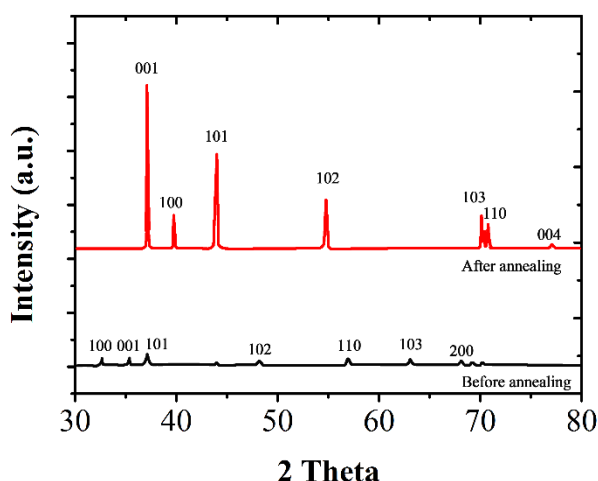


Figure 1. XRD pattern of (A) as-prepared ZnO film and (B) annealed ZnO film.

The crystallization of the specimen was proven, and when the calcination was completely finished, uniform lattice strain was acquired. There was a left shift in all peaks owing to the calcination process, which caused the higher density of the ZnO crystals. Moreover, the ZnO specimen has the

chemical formula ZnO (from the XRD test) and had a hexagonal crystal structure. The XRD pattern of the prepared specimen had all the diffraction peaks indexed similar to those found in the typical diffraction pattern of hexagonal phase ZnO, which is indicative of a wurtzite structure. In addition, compared with other ZnO samples, the diffraction intensity of the (001) plane was higher, revealing that the ZnO nanorods possessed a favorable orientation along the [001] direction (perpendicular to the cover of the substrate). Figure 2 demonstrates the morphologies of the prepared ZnO films with nanostructures. The entire surface of the ITO was overlaid by the complicated ZnO nanostructures that assembled themselves on the photocatalytic films. These ZnO nanostructures possessed higher surface energy and hence could serve as active centers for the nucleation of ZnO rods [29]. The SEM plot of the porous ZnO film in nanosheets was revealed in Figure 1. The nanosheets, with a thickness of approximately 100 nm, developed vertically on the ITO and became three-dimensional macroporous films through their own assembly. The diameter and depth of those characteristic pores were approximately 10–20 μm and 2–5 μm , respectively.

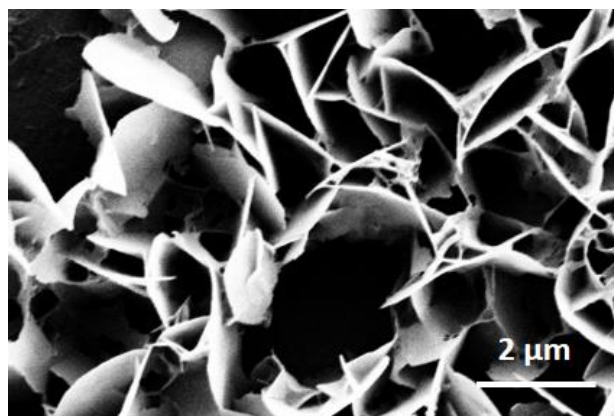


Figure 2. SEM plots of the as-prepared ZnO films with nanostructures

With the adoption of the MB degradation approach under ultraviolet radiation, the photocatalytic activities of the ZnO film prepared in this work and those of commercial and as-prepared ZnO were studied. The outstanding photocatalytic nature of ZnO was proven when the MB solution underwent nearly 80% degradation for 6 hours under UV radiation. It can be seen in Figure 3 that the ZnO film revealed greater photocatalytic activity in comparison with as-prepared ZnO whose MB concentration was reduced to 15% after 6 hours of irradiation. The decay that occurred in the MB solution can be attributed to an oxidation process that occurs on the ZnO surface through photogenerated holes. It is well-known that the quick recombination of photoinduced charge carriers is a main problem that restricts the photocatalytic performance of ZnO [30]. That is, there was an electron-hole pair when there was no light intensity. Under the UV radiation, the energy that was generated was greater than the ZnO band gap energy. As a result, electrons and holes were produced in the conduction and valence bands, respectively. Holes existing at the surface of the ZnO nanostructures react with water to give rise to extremely reactive hydroxyl radicals; meanwhile oxygen functions as a one-electron acceptor by becoming a superoxide radical anion originating from hydroxyl

radicals. Superoxide has an outstanding oxidation capacity and, thus, a high potential to degrade organic dye; in the disintegration of MB, the MB turns into carbon dioxide and water. The ZnO film, characterized by its high surface area and active light response, exhibited good photocatalytic properties. The catalytic performance of the ZnO film is compared with other catalysts in the literature in Table 1. The results indicate that our proposed ZnO film is a competitive catalyst with excellent catalytic performance.

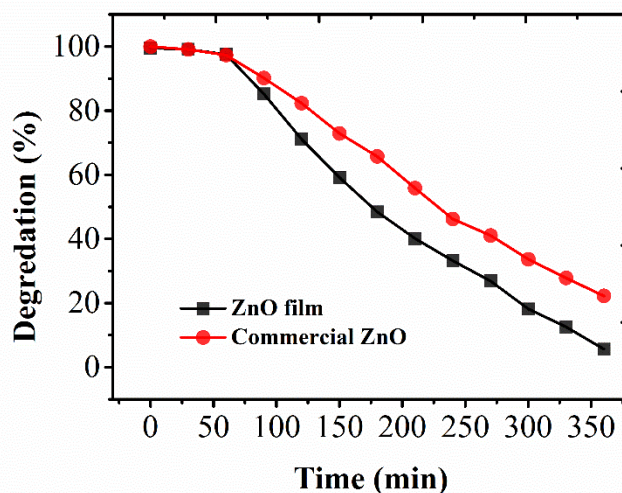


Figure 3. Light degradation of MB solution with ZnO film and commercial ZnO with increasing degradation time.

Table 1. MB-reduction performance comparison of the proposed ZnO film and other reported catalysts.

Catalyst	Rate constant (min^{-1})	Reference
Bimetallic Pt–Cu	2.7	[31]
Ag-Fe ₃ O ₄	0.42	[32]
Polydopamine microparticles	0.328	[33]
Sm-doped CeO ₂	0.161	[34]
BNNS-Au	0.064	[35]
ZnO film	0.122	This work

To evaluate the efficiency of the ZnO film photocatalytic activity, one scanning potentiostat was used that could measure the current (I) under an employed potential (V). With respect to the application to water electrolysis, efficiencies higher than 90% were revealed from -1 to 1 V. Then, with the purpose of mastering the efficiency of ZnO thin films toward water electrolysis, the specimens underwent evaluation and tests of their I-V features between -1 V and 1 V. Figure 4 demonstrates the characteristic V curves of the commercial ZnO and the prepared ZnO film in the presence of UV radiation, as well as the ZnO without radiation [36, 37]. The light current density J_p had a dramatic mean value of 17.14 mA/cm^2 for the ZnO film under UV radiation, in

comparison with 5.24 mA/cm^2 and 1.77 mA/cm^2 for the prepared ZnO with UV radiation and ZnO film without radiation, respectively. The contribution made by the catalytic activity can be seen in the discrepancies in light current density with or without the radiation. The enhancement of photocurrent can be ascribed to the concentration of photoinduced electron-hole pairs. More specifically, a Schottky junction is formed at the interface between the AgD and AgCl, resulting in charge transfer pathway [38]. Nevertheless, before the acquisition of the visible light spectrum (390–700 nm), when the spectral wavelength was improved, there was decline in the current density. The average J_p of 13.71 mA/cm^2 was found for the ZnO layer under visible light, as shown in Figure 5, and this value is bigger than those of both the prepared ZnO under the same conditions and the ZnO film without radiation, which were 2.19 mA/cm^2 and 1.51 mA/cm^2 , respectively.

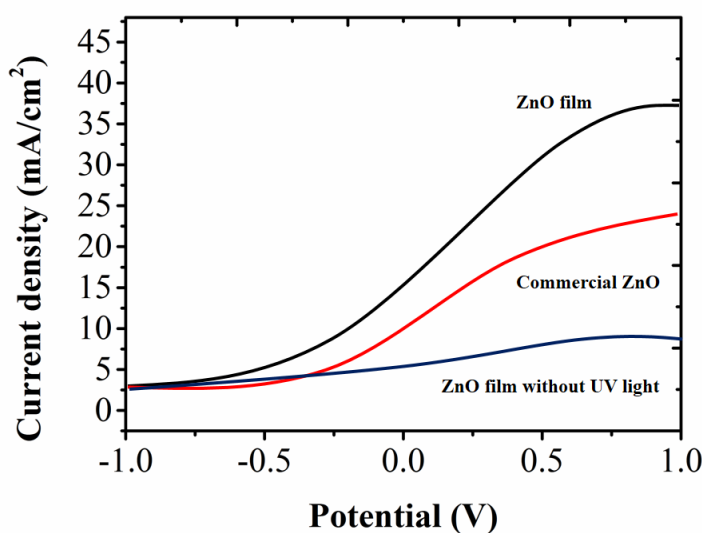


Figure 4. Current density-voltage features for commercial ZnO and the prepared ZnO films in the presence and absence of UV radiation.

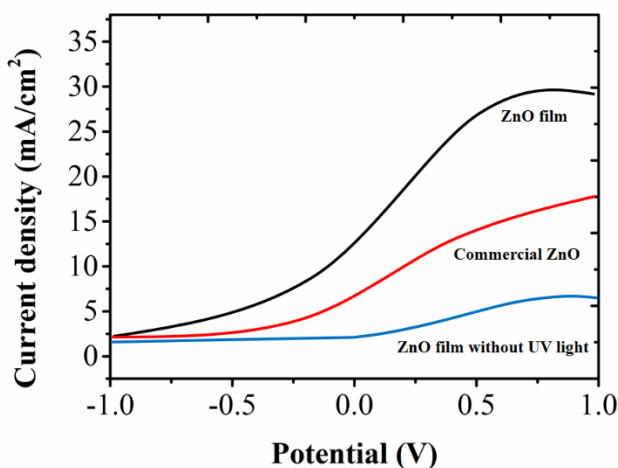


Figure 5. Current density-voltage features for commercial ZnO and the prepared ZnO films in the presence and absence of visible light.

According to the outcomes of typical J-V curves, the as-prepared ZnO film performed poorly, which was caused by the presence of oxygen vacancies within the bulk ZnO, indicating that the growing amount of recombination centers led to the decline of photoinduced e^- mobility. These centers originated from their integration with the Zn substrate owing to a sequence of resistances that resulted from growing trap states. In addition, the amorphous phase possessed many drawbacks, e.g., microspores and impurities, which function as the recombination centers and lead to a decline of J_p . It should be noted that, in general, the prepared ZnO film lacks the ability to form a regular depletion region. A moderate increase in the J_p of a hot-treated (600°C) ZnO specimen film, to 17.14 mA/cm², was found, indicating the positive effect of the crystal structure of the ZnO film in developing photocurrent. Moreover, the high specific surface area of the nanoarchitecture has a high potential to be a promoter of strong light scattering effects and incident ray absorption from any orientation. Within the electrolyte, the photoinduced electrons were formed due to the large active surface area, and they shifted to the substrate. With the employment of an external circuit, the light-induced electron transfers to the counter electrode and improves the photocatalytic activity and photoelectrochemical response dramatically.

4. CONCLUSIONS

In this study, with the adoption of an electrodeposition technique, a nanostructured ZnO film was formed on the ITO substrate under the calcination temperature of 600°C. On the basis of the characterization, it is revealed that the specimen can be regarded as a zinc oxide film with the chemical formula ZnO and has a hexagonal crystal structure. The photocatalytic experiments (light-current density and MB degradation) proved the fact that zinc oxide films possesses outstanding photocatalytic activity.

ACKNOWLEDGEMENT

This work was supported by Industrial Science and Technology Research of Shaanxi Province (2016GY-226, 2014K08-36), Science and Technology Bureau of Baoji (2013R7-4), Shaanxi Key Laboratory of Phytochemistry (14JS005.12JS008) and Baoji University of Arts and Sciences (ZK12033).

References

1. W. Liang, Y. Luo, S. Song, X. Dong and X. Yu, *Polymer Degradation & Stability*, 98 (2013) 1754.
2. X. Wang, H. Fan and P. Ren, *Catalysis Communications*, 31 (2013) 37.
3. K. Hayat, M. Gondal, M. Khaled, Z. Yamani and S. Ahmed, *J. Hazard. Mater.*, 186 (2011) 1226.
4. Q. Rahman, M. Ahmad, S. Misra and M. Lohani, *Mater. Lett.*, 91 (2013) 170.
5. W. Xu, S. Liu, S. Lu, S. Kang, Y. Zhou and H. Zhang, *Journal of Colloid & Interface Science*, 351 (2010) 210.
6. A. Xu, Y. Gao and H. Liu, *J. Catal.*, 207 (2002) 151.
7. J. Yu, Y. Su and B. Cheng, *Adv Funct Mater*, 17 (2007) 1984.
8. H. Yu, J. Yu, S. Liu and S. Mann, *Chemistry of Materials*, 19 (2007) 4327.

9. Z. Liu, R. Zhang, Q. Meng, X. Zhang and Y. Sun, *Medchemcomm*, 7 (2016)
10. L. Song, C. Kang, Y. Sun, W. Huang, W. Liu and Z. Qian, *Cellular Physiology & Biochemistry*, 40 (2016) 443.
11. H. Sun, J. Zhu, Y. Chen, Y. Sun, H. Zhi, H. Li and Q. You, *Chinese Journal of Chemistry*, 29 (2011) 1785.
12. M. Law, L. Greene, J. Johnson, R. Saykally and P. Yang, *Nature Materials*, 4 (2005) 455.
13. D. Banerjee, J. Lao, D. Wang, J. Huang, D. Steeves, B. Kimball and Z. Ren, *Nanotechnology*, 15 (2004) 404.
14. Y. Ding, P.X. Gao and Z.L. Wang, *Journal of the American Chemical Society*, 126 (2004) 2066.
15. J. Choy, E. Jang, J. Won, J. Chung, D. Jang and Y. Kim, *Adv. Mater.*, 15 (2003) 1911.
16. W. Hughes and Z. Wang, *Journal of the American Chemical Society*, 126 (2004) 6703.
17. W. Park, G. Yi, M. Kim and S. Pennycook, *Adv. Mater.*, 14 (2002) 1841.
18. C. Xu and X. Sun, *Applied Physics Letters*, 83 (2003) 3806.
19. A. Umar, M. Rahman, A. Al-Hajry and Y. Hahn, *Talanta*, 78 (2009) 284.
20. T. Zhang, W. Dong, M. Keeter-Brewer, S. Konar, R. Njabon and Z. Tian, *Journal of the American Chemical Society*, 128 (2006) 10960.
21. R. Wang, C. Liu, J. Huang, S. Chen, Y. Tseng and S. Kung, *Applied Physics Letters*, 87 (2005) 013110.
22. Z. Wang, X. Qian, J. Yin and Z. Zhu, *J. Solid State. Chem.*, 177 (2004) 2144.
23. C. Gouvea, F. Wypych, S. Moraes, N. Duran, N. Nagata and P. Peralta-Zamora, *Chemosphere*, 40 (2000) 433.
24. Y. Tong, J. Cheng, Y. Liu and G. Siu, *Scripta Materialia*, 60 (2009) 1093.
25. C. Ye, Y. Bando, G. Shen and D. Golberg, *J Phys Chem B*, 110 (2006) 15146.
26. T. Sounart, J. Liu, J. Voigt, M. Huo, E. Spoecker and B. McKenzie, *Journal of the American Chemical Society*, 129 (2007) 15786.
27. F. Zhao, X. Li, J. Zheng, X. Yang, F. Zhao, K. Wong, J. Wang, W. Lin, M. Wu and Q. Su, *Chemistry of Materials*, 20 (2008) 1197.
28. B. Lim, M. Jiang, J. Tao, P. Camargo, Y. Zhu and Y. Xia, *Adv Funct Mater*, 19 (2009) 189.
29. E. Rokhsat and O. Akhavan, *Appl. Surf. Sci.*, 371 (2016) 590.
30. L. Fu, G. Lai, H. Zhang and A. Yu, *Journal of Nanoscience and Nanotechnology*, 15 (2015) 4325.
31. H. Singh, N. Gupta, S. Sharma and R. Sharma, *Colloids and Surfaces A: Physicochemical and Engineering Aspects*, 416 (2013) 43.
32. L. Ai, C. Zeng and Q. Wang, *Catalysis Communications*, 14 (2011) 68.
33. S. Du, Z. Liao, Z. Qin, F. Zuo and X. Li, *Catalysis Communications*, 72 (2015) 86.
34. S. Kundu, N. Sutradhar, R. Thangamuthu, B. Subramanian, A. Panda and M. Jayachandran, *Journal of Nanoparticle Research*, 14 (2012) 1.
35. L. Fu, G. Chen, N. Jiang, J. Yu, C. Lin and A. Yu, *Journal of Materials Chemistry A*, 4 (2016) 19107.
36. S. Licht, B. Wang, S. Mukerji, T. Soga, M. Umeno and H. Tributsch, *J Phys Chem B*, 104 (2000) 8920.
37. S. Licht, B. Wang, S. Mukerji, T. Soga, M. Umeno and H. Tributsch, *International Journal of Hydrogen Energy*, 26 (2001) 653.
38. L. Fu, A. Wang, Y. Zheng, W. Cai and Z. Fu, *Mater. Lett.*, 142 (2015) 119.